Electronic Supplementary Material (ESI) for Lab on a Chip.

Supplementary Material

Ultra-fast, sensitive and low-cost real-time PCR system for nucleic acid detection

Shaolei Huang,[abcd] Yiquan An,[acd] Bangchao Xi,[acd] Xianglian Gong,[acd] Zhongfu Chen,[acd] Shan Shao,[acd] Shengxiang Ge,[acd] Jun Zhang,[acd] Dongxu Zhang, *[abcd] and Ningshao Xia *[abcd]

[a.] *School of Public Health, Xiamen University, Fujian, China.*

[b.] *Discipline of Intelligent Instrument and Equipment.*

[c.] *National Institute of Diagnostics and Vaccine Development in Infectious Diseases (Xiamen University), Fujian, China.*

[d.] *State Key Laboratory of Molecular Vaccinology and Molecular Diagnostics, Fujian, China.*

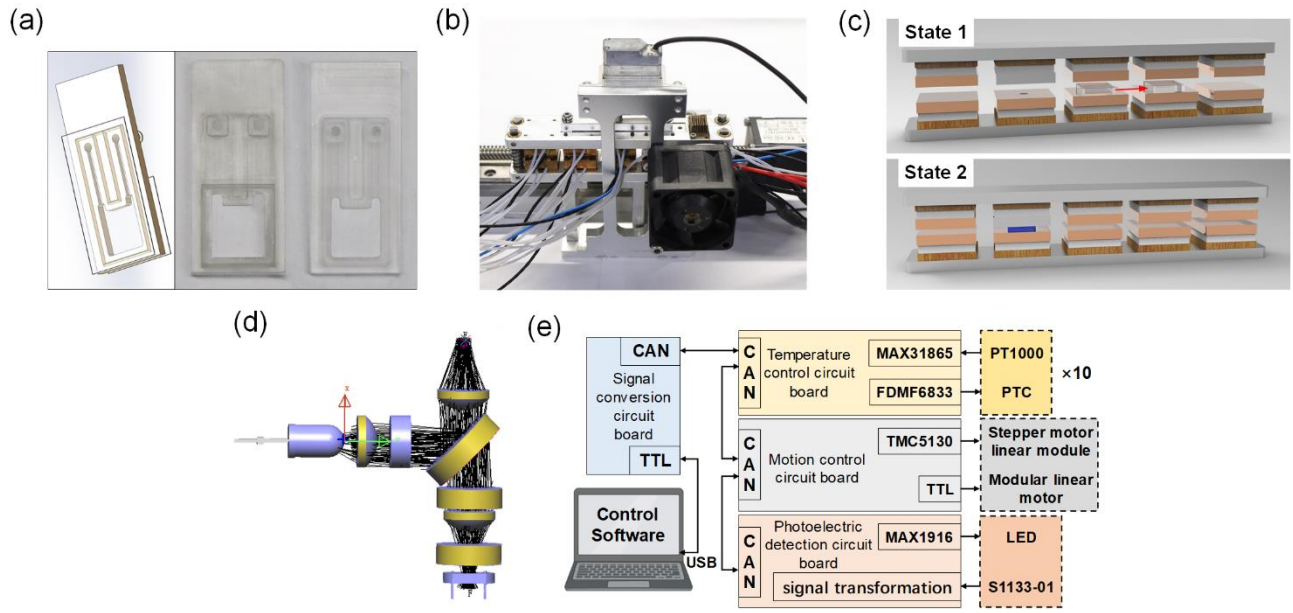

Fig. S1 Schematic diagram of the microfluidic chip and real-time PCR device. (a) Microfluidic chip 3D rear view (showing microfluidic channels) and CNC machined microfluidic chip (front and back). **(b)** Rear view of the real-time PCR device (including cooling fan). **(c)** Two states of the microfluidic chip and amplification module cooperation. State 1: Microfluidic chip moves between different temperature-zones. State 2: The heat-conducting blocks clamp the microfluidic chip for fast heat transfer and fluorescence detection. **(d)** The optical simulation uses Light tools software to determine each optical element's spatial location and distance. **(e)** The electronic control system consists of the communication protocols between the modules and the main driver chips used.

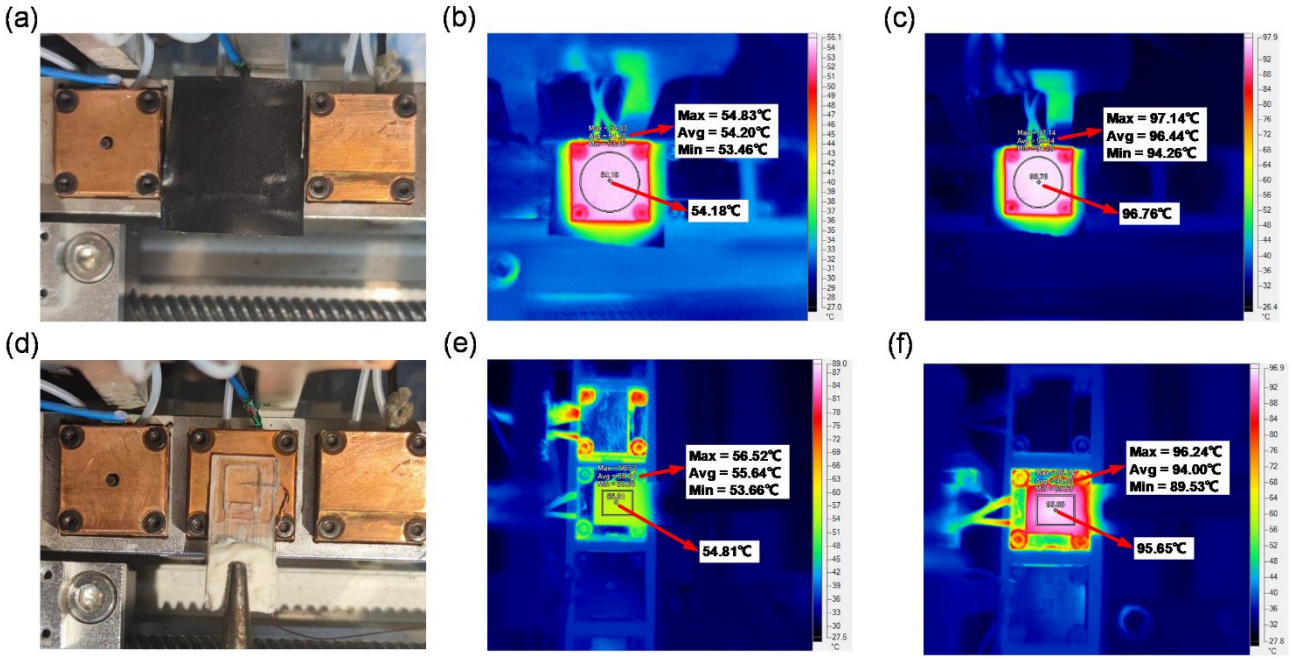

Fig. S2 Thermal map of the microfluidic chip and heat-conducting block under different conditions. (a) Heat-conducting block with black high-temperature tape on the surface for infrared temperature measurement. **(b)** Thermal map of heat-conducting block under low-temperature conditions. **(c)** Thermal map of heat-conducting block under high-temperature conditions. **(d)** The microfluidic chip under single-sided heating conditions. **(e)** Thermal map of the microfluidic chip under low-temperature conditions. **(f)** Thermal map of the microfluidic chip under high-temperature conditions.

The "sandwich" structure of this system makes it difficult to measure the overall thermal map of the microfluidic chip and heat-conducting block directly, so we measured the thermal map using an infrared camera when only one side of the microfluidic chip was heated. Since the surface of the heat-conducting block is relatively rough, resulting in a large difference in reflectance, a layer of black high-temperature tape was applied to the surface of the heat-conducting block to measure its temperature. The infrared images showed that the temperature in the center of the liquid inside the microfluidic chip could basically represent the temperature of the whole liquid more accurately. In addition, since one side of the microfluidic chip was exposed to air, the temperature uniformity of the liquid inside the chip is more affected by this under high-temperature conditions, while the actual "sandwich" structure would have better temperature uniformity than the current test conditions, so measuring the temperature of the center by a thermocouple can meet the test requirements of this system.

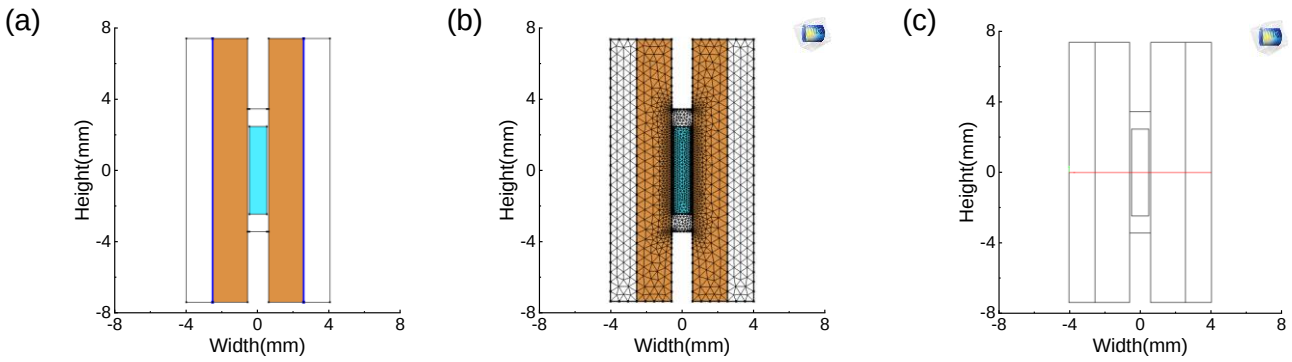

Fig. S3 Heat transfer simulation model. (a) Establishing a simplified two-dimensional simulation model in COMSOL. **(b)** The meshing of the simulation model. **(c)** Setting up the two-dimensional section line passing through the center of the liquid in the simulation model.

Two basic assumptions for building a simplified two-dimensional simulation model: (1) Although the microfluidic chip would bring about temperature fluctuations in the heat-conducting blocks when it moved among temperature-zones, the small temperature fluctuations have a negligible impact on the temperature change of the liquid inside the chip due to the large thermal capacity of the heat-conducting blocks and the low thermal conductivity of the PC material and can be ignored. (2) The chip was moved and pressed under the action of the motor, and this process would impact the temperature change of the liquid but can be ignored when exploring the impact of the following key factors. The two-dimensional simulation model was based on the central section of the liquid, and the corresponding temperature boundary conditions were imposed.

The chamber lengths were set to 3 mm, 5 mm, and 7 mm for the 9 μL, 25 μL, and 49 μL sample volumes conditions, and the chamber widths were set to 0.5 mm, 1 mm, and 2 mm for the conditions of different heat transfer specific surface areas.

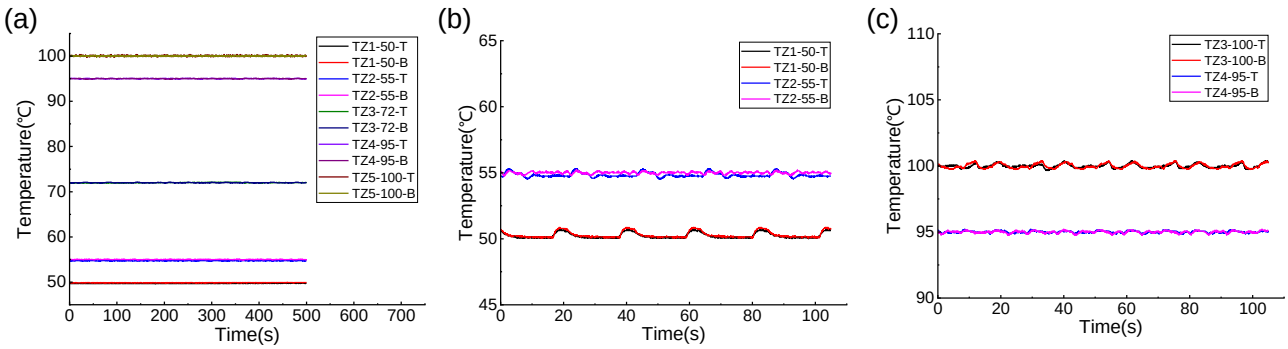

Fig. S4 Results of thermodynamic performance testing. (a) Temperature change curves of each heat-conducting block when PCR experiment was not performed. **(b)** Temperature change curves of the low-temperature heat-conducting block when the PCR experiment was performed. **(c)** Temperature change curves of high-temperature heat-conducting block when PCR experiment was performed. The testing was based on the following conditions: high-temperature overshoot was set to 100°C, low-temperature overshoot was set to 50°C, and the dwell times of denaturation, extension, and annealing stages were set to 5s, 2s, and 10s in that order. Explanatory notes for TZ1-50-T. TZ1: Temperature-zone 1. 50: Set the temperature to 50°C. T: Top heat-conducting block. B: Bottom heat-conducting block.

Tab. S1 Temperature of each heat-conducting block when PCR experiment was not performed and when PCR experiment was performed.

PCR experiment was not performed			PCR experiment was performed		
Temperature	upper part (℃)	lower part (℃)	Temperature	upper part (℃)	lower part (℃)
Zone1-50℃	49.87±0.12	49.70±0.13	Zone1-50℃	50.15±0.71	50.11±0.59
Zone2-55℃	55.00±0.09	54.73±0.10	Zone2-55℃	54.75±0.55	55.00±0.25
Zone3-72℃	72.00±0.17	72.00±0.15	Zone3-95℃	95.00±0.23	95.00±0.25
Zone4-95℃	95.00±0.17	95.00±0.17	Zone4-100℃	100.00±0.38	100.00±0.38
Zone5-100℃	100.05±0.32	100.08±0.35			

When the PCR experiment was not performed, the temperature fluctuations of each heat-conducting block were small, but the temperature fluctuations of the temperature-zone set to 100°C were relatively large, mainly due to the larger convective heat exchange between the blocks and the external environment. When the PCR experiment was performed, the temperature fluctuations of the temperature-zones set to 50°C and 100°C were large, mainly because these two temperature-zones buffer most of the energy changes of the microfluidic chip. It was also found that the temperature fluctuations of the upper part of the heat-conducting block set to 55°C were also large, mainly because the heat-conducting copper block was replaced with an aluminum block, whose reduced heat capacity brought about a larger fluctuation in temperature. The aluminum block has a stronger light reflection ability, which can enhance the sensitivity of fluorescence detection.

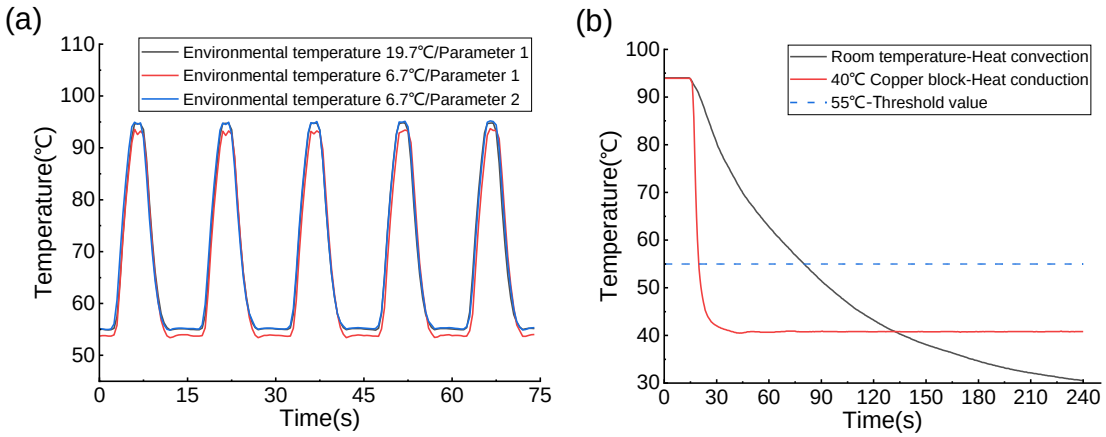

Fig. S5 Influence of external environment on the system. (a) Temperature change curves of the liquid inside the microfluidic chip when the external temperature environment changes. **(b)** Temperature change curves when the liquid inside the microfluidic chip was cooled down under different conditions.

In order to evaluate the degree of influence of external temperature changes on the system, we conducted relevant tests under room temperature conditions and in a 4°C cold room, and the actual measured indoor temperature was about 19.7°C, and the temperature in the 4°C cold room was about 6.7°C. We first set the temperature values of each temperature zone to 40°C, 55°C, 95°C and 110°C under the indoor temperature condition and adjusted the operation timing of the system to achieve a better temperature control effect on the liquid inside the microfluidic chip. Then, we moved the whole experimental equipment to the 4°C cold room to monitor the temperature change of the liquid inside the chip, and it can be found that the actual temperature of the liquid differed from the target temperature by about 1.2°C during the denaturation and annealing stages, proving that the system receives the influence of external temperature. Finally, we adjusted the temperature values of each temperature zone and set them to 41°C, 56°C, 96°C and 111°C in turn, and the adjusted temperature change curve of the liquid was basically consistent with the room temperature conditions. The above experiments prove that our system will be affected by the external temperature but can be adjusted by certain parameters to achieve stable operation of the system in different external environments.

We measured the cooling rate of the liquid inside the chip at room temperature (~26°C) and at double-sided heat-conducting blocks clamping (~40°C) to demonstrate the necessity of setting up a temperature zone far below the annealing temperature. We first heated the liquid inside the chip to denaturation temperature and then cooled down the liquid under the above two conditions. The liquid cooled down to 55°C for about 4 s under 40°C heat-conducting blocks, while the liquid cooled down to 55°C for about 64 s under room temperature. We set up a temperature zone far below the annealing temperature so that the chip was in direct contact with the heat-conducting blocks at a temperature of 40°C, and the heat transfer type is heat conduction, while the chip is placed at room temperature (~26°C) for cooling, and the heat transfer type is heat convection. According to Fourier's law and Newton's cooling equation, although the temperature difference of the latter is larger, the former has a greater heat transfer rate and can provide a higher cooling rate considering factors such as thermal conductivity and convective heat transfer coefficient.

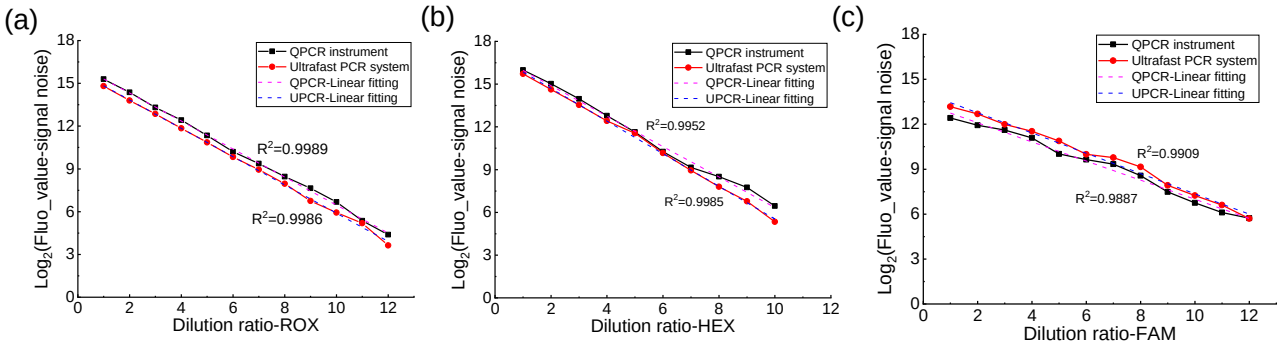

Fig. S6 Results of fluorescence detection performance testing. (a) Gradient fluorescent dye testing of ROX. **(b)** Gradient fluorescent dye testing of HEX. **(c)** Gradient fluorescent dye testing of FAM.